Carboxylic Acid-Catalyzed Controlled Ring-Opening Polymerization of Sarcosine *N*-Carboxyanhydride: Fast Kinetics, Ultra-High Molecular Weight, and Mechanistic Insights

Shuo Wang[1], Ming-Yuan Lu[1], Si-Kang Wan[2], Chun-Yan Lyu[1], Zi-You Tian[1], Kai Liu[2], and Hua Lu[1]*

[1]Beijing National Laboratory for Molecular Sciences, Center for Soft Matter Science and Engineering, Key Laboratory of Polymer Chemistry and Physics of Ministry of Education, College of Chemistry and Molecular Engineering, Peking University, Beijing 100871, China

[2]Engineering Research Center of Advanced Rare Earth Materials (Ministry of Education), Department of Chemistry, Tsinghua University, 100084 Beijing, China

Corresponding Author: chemhualu@pku.edu.cn (H.L.)

ABSTRACT: The rapid and controlled synthesis of high molecular weight (MW) polysarcosine (pSar), a potential polyethylene glycol (PEG) alternative, via the ring-opening polymerization (ROP) of *N*-carboxyanhydride (NCA) is rare and challenging. Here, we report carboxylic acid-catalyzed well-controlled ROP of Sar-NCA, which accelerates the polymerization rate up to 50 times, and enables the robust synthesis of pSar with unprecedented high molecular weight (MW) up to 586 kDa (DP ~ 8200) and exceptionally narrow dispersity (*Đ*) below 1.02. Density functional theory (DFT) calculations combined with mechanistic experiments identify the carbamic acid as dormant species before generating the secondary amine for chain propagation, and elucidate the role of carboxylic acid as a bifunctional catalyst that significantly facilitates proton transfer processes and avoids charge separation. High MW pSar demonstrates improved thermal and mechanical properties over low MW pSar. This work provides a simple yet highly efficient approach to ultra-high MW pSar and generates new fundamental understandings useful not only for the ROP of Sar-NCA but also other NCAs.

1. Background

Polysarcosine (pSar) is a non-ionic water-soluble polypeptoid with the biogenic amino acid sarcosine (*N*-methylglycine) as the repeating unit. Being comparable in flexibility, hydrophilicity, low cytotoxicity, and excellent anti-biofouling properties to polyethylene glycol (PEG), pSar has been considered a potential alternative to PEG.[1-3] For example, the pSar-interferon conjugate exhibits a similar in vivo circulation half-life to the PEG-interferon conjugate of the same size while being more potent in inhibiting tumor growth.[4] pSar-functionalized nanoparticles (LNPs) have also been reported for mRNA delivery, which led to lower immunogenicity and higher delivery efficiency over conventional PEGylated LNPs.[5,6] Additionally, pSar has been frequently used as the hydrophilic composition of nonionic surfactants or amphiphilic block copolymers for the purpose of disease diagnosis and treatment.[7-14]

pSar is typically synthesized through the ring-opening polymerization (ROP) of sarcosine *N*-carboxyanhydride (Sar-NCA)[15-30] or *N*-thiocarboxyanhydride (Sar-NTA).[31-36] However, existing Sar-NCA polymerization methods often require strictly anhydrous conditions, limiting its broader applications and large-scale production. In contrast, Sar-NTA demonstrates better moisture tolerance than Sar-NCA but suffers harsh polymerization conditions due to lower reactivity.[32] Furthermore, the achievable molecular weight (MW) of pSar via current methods is generally limited, with degrees of polymerization (DP) lower than 500 and a maximal MW of ~35 kDa.[34] As several FDA-approved PEGylated protein drugs are modified with PEG of 40-80 kDa,[37] it is crucial to develop a rapid and robust Sar-NCA polymerization method capable of achieving a broader and higher MW coverage.

The elucidation of the polymerization mechanism plays a pivotal role in the development of new methodologies.[38] In the case of the ROP of Sar-NCA initiated by primary amines, the chain propagation involves two consecutive steps: the ring-opening amidation reaction wherein the amine attacks the carbonyl group of NCA, and the subsequent decarboxylation reaction of the carbamic acid intermediate (Figure 1A).[21] However, insights into the reaction details, such as the proton transfer process[39] and rate-determining step (RDS), were surprisingly rare.[40] Essentially, proton transfer is crucial in both the amidation and decarboxylation processes but often faces geometric constraints in intramolecular cases, leading to high activation energies due to unfavorable transition states (TS).[41,42] On the other hand, intermolecular proton transfer catalysts can overcome the geometric constraints limitations and reduce activation energy.[43-47] In a recent work on the ROP of proline NCA (Pro-NCA), Lu *et al.* noticed a remarkable acceleration effect by simply adding water as the co-solvent.[48] Through experiments and density functional theory (DFT) calculations, they ascribed this unexpected acceleration to water's ability to act as a proton shuttle, which effectively lowered the energy barriers. Yet, this water-accelerating effect has not been observed in the ROP of other NCA.

Carboxylic acids are common proton transfer catalysts, possessing both an acidic proton donor site and a basic carbonyl proton acceptor site within a conjugated π system.[49,50] This enables the carboxylic group to accept an external proton and donate its own proton via a concerted TS without compromising electronic neutrality.[51-53] In this regard, we envision that introducing carboxylic acids as proton transfer catalysts into the ROP of Sar-NCA holds great potential for enhancing the polymerization rate. In an early study conducted by Bamford et al. in 1954, the addition of pyridine-2-carboxylic acid to the ROP of Sar-NCA in nitrobenzene was found to

increase the polymerization rate by ~0.5 times (Figure 1B).[54] Although this work had a limited polymerization rate and lacked characterization on molecular weight distribution (MWD) of the pSar product, it did provide the first experimental evidence supporting the use of carboxylic acids in NCA polymerization. More recently, both the Zhang[36] and Ling[34] labs reported the carboxylic acid-promoted ROP of NTA and *N*-substituted NTA, respectively (Figure 1B). Remarkable rate acceleration was observed in both ROP systems after adding carboxylic acids, which was attributed to the promoted removal of carbonyl sulfide. Furthermore, we recently discovered that the addition of benzoic acid in the ROP of unprotected penicillamine NCA (Pen-NCA) not only accelerated the polymerization rate but also improved the selectivity of polymerization over monomer isomerization (Figure 1B).[55] These successes motivated us to further investigate the role of carboxylic acids in the polymerization process of Sar-NCA.

Herein, we report a systematic study on carboxylic acid-catalyzed primary amine-initiated well-controlled ROP of Sar-NCA. The system enables the fast and robust synthesis of pSar with unprecedented high MW up to 586 kDa (DP ~ 8200), 16 times higher than the previous record, and exceptionally narrow dispersity ($Đ$) below 1.02 (Figure 1C). Moreover, the polymerization can be carried out under mild and ambient conditions without dry solvents, Schlenk line, or glove box operations. DFT calculations combined with mechanistic experiments show that the ring-opening step of carboxylic acid-catalyzed Sar-NCA ROP proceeds through a stepwise nucleophilic addition-elimination process, with the elimination of the tetrahedral intermediate—rather than the nucleophilic addition—as the rate-determining step. The carboxylic acid reduces the charge separation during the reaction through hydrogen-bond bridging and assists the proton transfer process in the form of a proton shuttle. High-molecular-weight pSar shows excellent

thermal stabilities and good processibility to form high-strength transparent films.

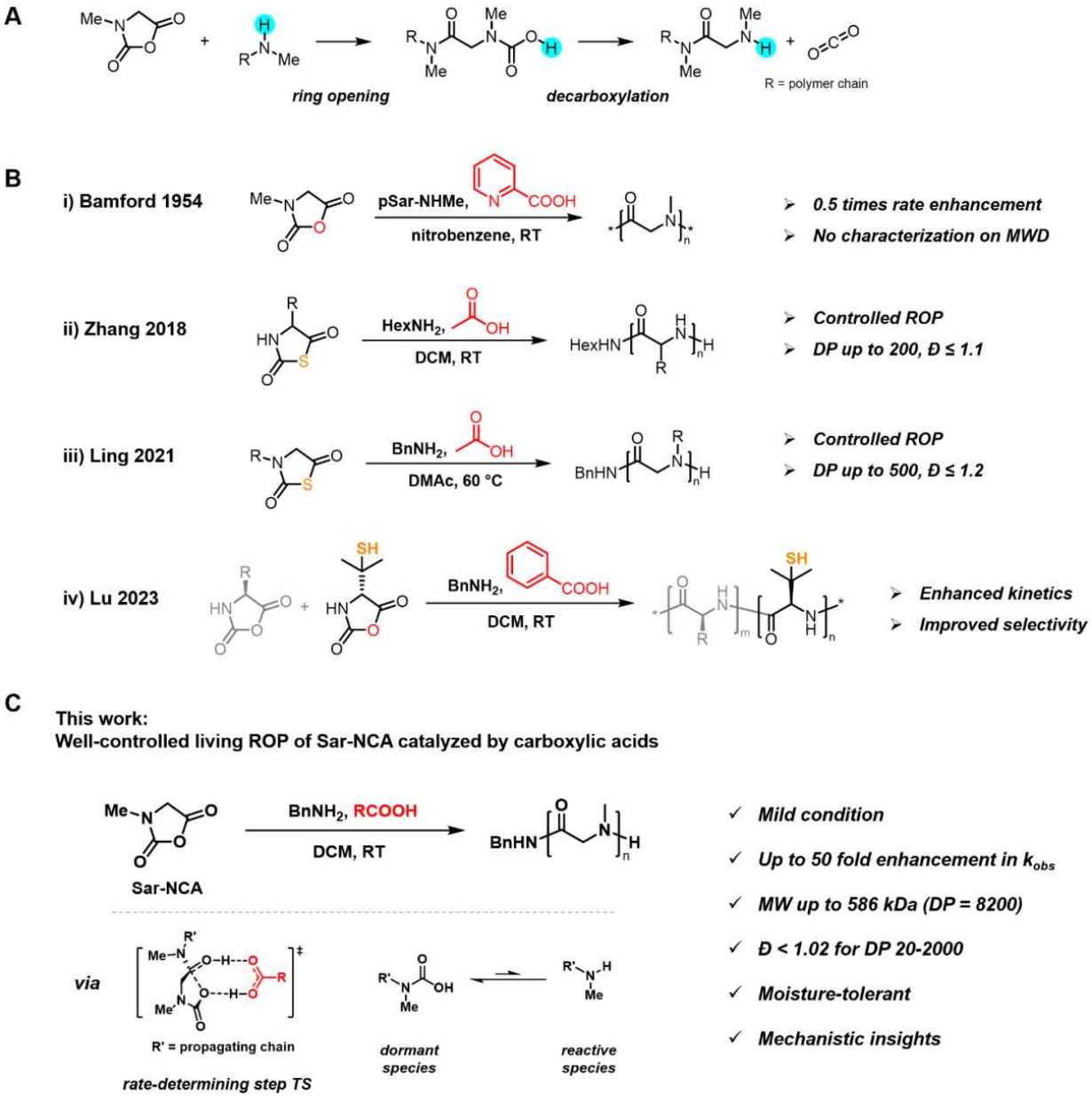

Figure 1. (A) Two consecutive steps for chain propagation of Sar-NCA ROP. (B) Previous works on carboxylic acid-catalyzed ROP of NCAs or NTAs. (C) Carboxylic acid-catalyzed ROP of Sar-NCA studied in this work.

2. Results and discussion

2.1 Benzoic acid-catalyzed ROP of Sar-NCA

In our initial attempt, benzoic acid was used as the catalyst, and the benzylamine-mediated ROP of Sar-NCA was performed in dry dichloromethane (DCM) in a glove box at room temperature. At an initial monomer concentration ($[M]_0$) of 0.2 M, we found that the reaction system with a feeding $[M]_0/[I]_0/[A]_0$ (the initial concentration of monomer, initiator, and carboxylic acid catalyst, respectively) ratio of 50/1/5 achieved complete monomer conversion within 15 min (monitored by infrared spectroscopy); in contrast, the control group without benzoic acid required 2 h to reach a full conversion (Table 1, entry 1&3). Size exclusion chromatography (SEC) characterization of the acid-catalyzed polymerization exhibited a sharp and symmetrical peak (Figure 2A) with narrow dispersity of 1.01 and an obtained number-average molecular weight (M_n^{obt}) of 4.3 kDa, close to the calculated theoretical M_n (M_n^{cal} 3.7 kDa). Matrix-assisted laser desorption time-of-flight (MALDI-TOF) mass spectrometry confirmed the good end group fidelity of the acid-catalyzed polymerization, with the α- and ω-end of the pSar product (Table 1, entry 3) exclusively in the form of $C_6H_5CH_2NH$- and *H*-, respectively (Figure 2B).

With the encouraging initial results, we conducted systemic ROP studies with different $[M]_0/[I]_0$ ratios ranging from 20/1 to 1000/1 at a fixed $[I]_0/[A]_0$ ratio of 1/5, which all gave excellent results with $Đ$ below 1.02 and linearly increased M_n^{obt} close to M_n^{cal} (Table 1, entry 2-7; Figure 2C&2D). Raising $[M]_0$ from 0.2 to 0.4 M effectively accelerated the reaction without losing control over MW (Table 1, entry 7&8). Notably, under the catalysis of benzoic acid, the polymerization with $[M]_0/[I]_0$ of 2000 was completed within 2.5 h, producing pSar with M_n^{obt} of 136.9 kDa (M_n^{cal} = 142.3 kDa) and $Đ$ <1.01 (Table 1, entry 10); in contrast, the same reaction without acid catalysis rendered only ~75% monomer conversion even after overnight reaction, affording pSar with a severely lower M_n^{obt} and a tailing SEC trace (Table 1, entry 11; Figure S1). At a further increased $[M]_0/[I]_0$ of 5000, remarkably, the polymerization still maintained excellent

control (M_n^{obt} 369.7 kDa vs. M_n^{cal} 355.5 kDa, $Đ$ = 1.19) with a completed monomer conversion in 16.5 h (Table 1, entry 12). The upper limit of the system was finally reached at a $[M]_0/[I]_0$ of 10000/1 ($[M]_0$= 0.8 M), producing pSar after overnight reaction with a M_n^{obt} of 414.1 kDa, significantly lower than the M_n^{cal} of 710.9 kDa (Table 1, entry 13). This deviation could be attributed to the trace impurities in the reaction system. To the best of our knowledge, the rapid and controlled synthesis of pSar with DP of 600-5000 has never been reported.

Table 1. Benzoic acid-catalyzed ROP of Sar-NCA[a]

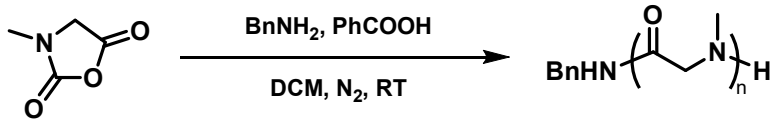

Sar-NCA

entry	$[M]_0$	$[M]_0/[I]_0/[A]_0$	time	M_n^{cal} (kDa)[b]	M_n^{obt} (kDa)[c]	$Đ$[c]
1	0.2 M	50/1/0	2 h	3.7	5.2	1.01
2	0.2 M	20/1/5	< 15 min	1.5	1.6	< 1.01
3	0.2 M	50/1/5	< 15 min	3.7	4.3	1.01
4	0.2 M	100/1/5	< 15 min	7.2	8.9	< 1.01
5	0.2 M	200/1/5	17 min	14.3	17.5	1.01
6	0.2 M	500/1/5	< 1.5 h	35.6	41.6	1.01
7	0.2 M	1000/1/5	2.5 h	71.2	74.3	< 1.01
8	0.4 M	1000/1/5	1.5 h	71.2	78.6	1.01
9	0.4 M	1500/1/5	1.5 h	106.7	111.8	< 1.01
10	0.4 M	2000/1/5	2.5 h	142.3	136.9	< 1.01
11	0.4 M	2000/1/0	13 h	142.3	84.5	1.14
12	0.4 M	5000/1/5	16.5 h	355.5	369.7[d]	1.19[d]
13	0.8 M	10000/1/5	16.5 h	710.9	414.1[d]	1.31[d]

[a]Conversions of monomer were monitored by infrared spectroscopy (IR) and were all above 95% except entry 11. [b]Calculated number-average molecular weight based on feed ratios. [c]Determined by SEC equipped with a multi-angle laser light scattering (MALLS) detector using dimethyl formamide containing 0.1 M LiBr as the mobile phase; dn/dc (658 nm) value of pSar was measured as 0.079 mL/g. [d]Determined by SEC relative to polystyrene standards.

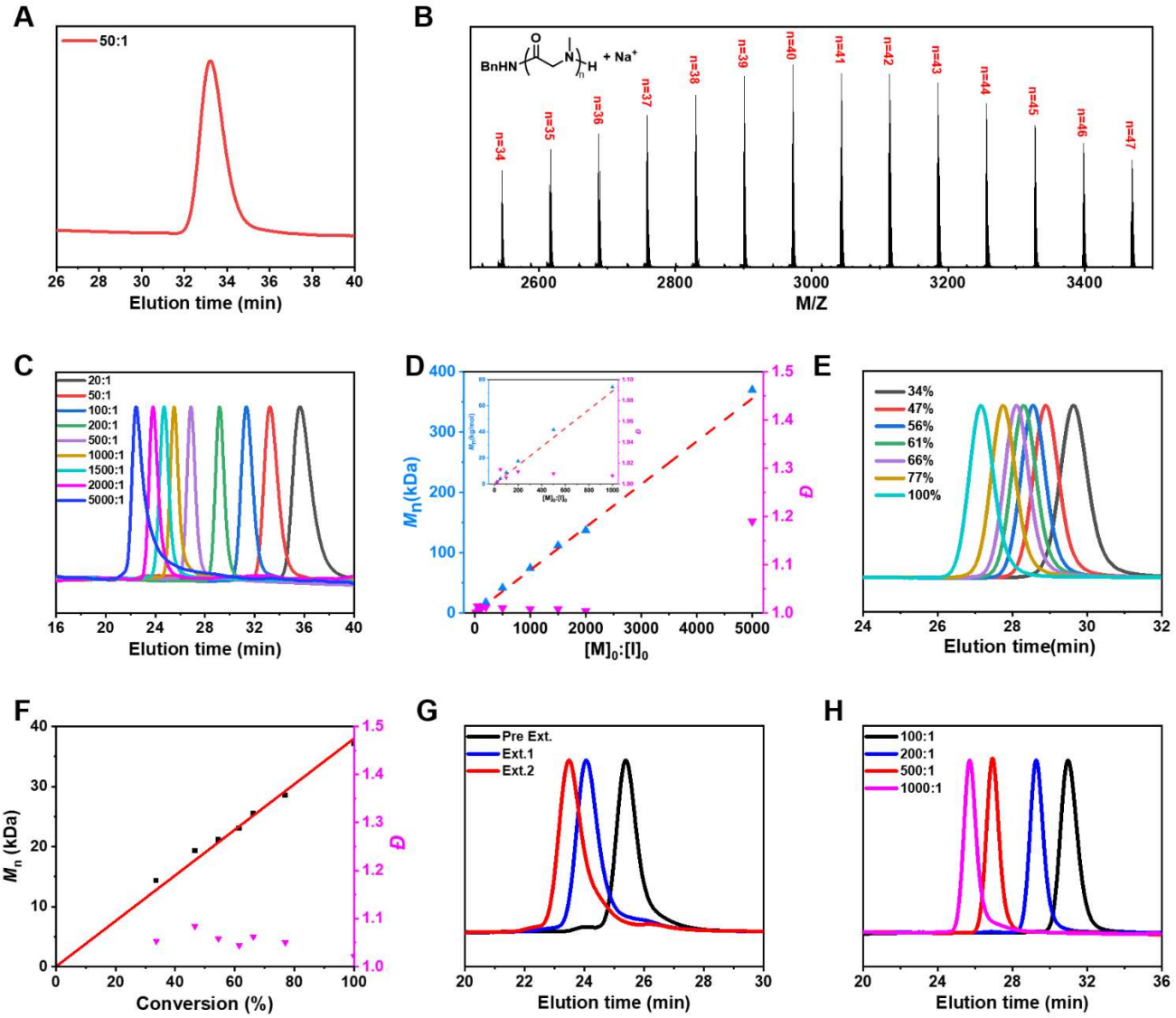

Figure 2. Benzoic acid-catalyzed ROP of Sar-NCA. (A) SEC trace of pSar at the $[M]_0/[I]_0/[A]_0$ ratio of 50/1/5. (B) MALDI-TOF MS spectrum of pSar prepared by $[M]_0/[I]_0/[A]_0$ = 50/1/5. (C)SEC traces of pSar at different $[M]_0/[I]_0$ ratios with $[I]_0/[A]_0$ fixed at 1/5. (D) Plots of M_n and $Đ$ as a function of the $[M]_0/[I]_0$ ratio. (E) SEC traces at different monomer conversions at the $[M]_0/[I]_0/[A]_0$ ratio of 500/1/5. (F) Plots of M_n and $Đ$ as a function of the monomer conversion at the $[M]_0/[I]_0/[A]_0$ ratio of 500/1/5. (G) SEC traces of pSar before and after chain extension. (H) SEC traces at different $[M]_0/[I]_0$ ratios in conventional DCM in ambient atmosphere.

Next, we examined the living character, i.e. chain growth pattern and chain extension, of the

benzoic acid-catalyzed ROP of Sar-NCA. At a $[M]_0/[I]_0/[A]_0$ ratio of 500/1/5, the M_n^{obt} of pSar was found to increase linearly with monomer conversion, which was consistent with the characteristics of controlled chain growth polymerization (Figure 2E&2F). Furthermore, to a fully converted $[M]_0/[I]_0/[A]_0$ ratio of 1000/1/5 system (Figure 2G, Pre-Ext, M_n^{obt} 76.7 kDa vs. M_n^{cal} 71.2 kDa, $Đ$ = 1.01), adding another 1000 equivalents of monomer reached full conversion within 4 h, with the SEC characterization revealed a complete shift of the product peak toward higher MW region (Figure 2G, Ext.1, M_n^{obt} 139.3 kDa vs. M_n^{cal} 142.3 kDa, $Đ$ = 1.02). The same chain extension could be repeated with good control of MW& $Đ$ (Figure 2F, Ext.2, M_n^{obt} 192.8 kDa vs. M_n^{cal} 213.3 kDa, $Đ$ = 1.01). Interestingly, when the polymerization was carried out under ambient conditions using HPLC-grade DCM, the controlled MWs were still observed, indicating good moisture and oxygen tolerance upon enhanced reaction rate (Figure 2H, Table S1).

To investigate the kinetic characters and details of the above benzoic acid-catalyzed ROP, an online Fourier transform infrared (FT-IR) spectrometer was employed to monitor monomer conversions in situ (Figure S2 and S3). First, the $[M]_0/[I]_0$ ratio was fixed at 200/1, and control experiments were conducted for polymerization systems with and without the addition of an acid catalyst. Under the same conditions, the ROP with a $[M]_0/[I]_0/[A]_0$ ratio of 200/1/5 reached 95% conversion within 17 min, while the reaction at the $[M]_0/[I]_0/[A]_0$ ratio of 200/1/0 took 5 h (Figure 3A). The 200/1/5 group presented typical first-order kinetics, and $\ln([M]_0/[M])$ had a good linear relationship with the reaction time (R^2 = 0.9989), through which the apparent first-order rate constant k_{obs} was calculated as $(30.9 \pm 0.3) \times 10^{-4}$ s^{-1} (Figure 3B). In contrast, the 200/1/0 group showed a slow, multi-stage kinetic profile that cannot be fitted with a simple kinetic equation (Figure S4). Next, $[I]_0$ was varied to probe the relationship between k_{obs} and $[I]_0$, and all the ROPs

were found to present typical first-order kinetics (Figure 3C, $R^2 > 0.998$). Plotting lg(k_{obs}) as a function of lg($[I]_0$) revealed a linear correlation with a slope of 1.3 ($R^2 = 0.988$), implying first-order dependence on $[I]_0$ (Figure 3C&D, Table S2). The change of reaction rate with $[A]_0$, however, was not monotonic (Figure 3E&F, Table S2). With $[A]_0$ increased, k_{obs} first increased, reaching a maximum of $(33.1 \pm 0.2) \times 10^{-4}$ s^{-1} at the $[I]_0/[A]_0$ ratio of 1/3, and then slowly decreased with further added $[A]_0$. Excessive carboxylic acid likely decreased the ROP rate through the competing reaction by partially protonating the chain propagating amine. Similar effects were seen in cases where strong acids such as HCl, HBF_4, and phosphoric acids were used for controlled ROP of NCAs by forming the amine-ammonium equilibrium, leading to significantly sacrificed reactivity, monomer conversion, and/or long induction period.[23,25,56] The acid-catalyzed ROP was also investigated in various solvents such as (deuterated) chloroform, nitrobenzene, acetonitrile, DMF, and DMSO at the feeding $[M]_0/[I]_0/[A]_0$ ratio of 200/1/5 (Table S3). The reactions displayed first-order kinetics in all solvents, among which chloroform showed comparable k_{obs} with DCM of $(27.6 \pm 0.2) \times 10^{-4}$ s^{-1}. The ROP rates in nitrobenzene and acetonitrile, however, were substantially slower with the k_{obs} being ~6×10^{-4} s^{-1}, one-fifth of that of DCM. ROP in DMF and DMSO demonstrated the slowest rates, with the k_{obs} of $(0.923 \pm 0.004) \times 10^{-4}$ s^{-1} and $(0.230 \pm 0.004) \times 10^{-4}$ s^{-1}, respectively. Interestingly, there was a strong negative correlation between k_{obs} and the Kamlet–Abboud–Taft basicity parameter β[57-59] of the solvents: the larger the β, the slower the reaction rate (Figure 3H). Since β was known as the ability to accept hydrogen bonds, the solvents with a strong Lewis basicity (greater β) tended to compete with substrates interacting with carboxylic acid catalysts via hydrogen bonding, thereby reducing the catalytic activity. The SEC traces of pSar obtained in chloroform, nitrobenzene, and acetonitrile were all symmetric and narrowly distributed, with the M_n^{obt} of pSar obtained in

nitrobenzene and acetonitrile showing greater coincidence with M_n^{cal} than that in chloroform. A severe tailing in the SEC peak was observed for the ROP in DMF, and the reaction in DMSO produced pSar with a much smaller M_n^{obt} than expected (Figure 3I, Table S3). Overall, DCM is the best solvent, with the fastest kinetics and excellent control on MW.

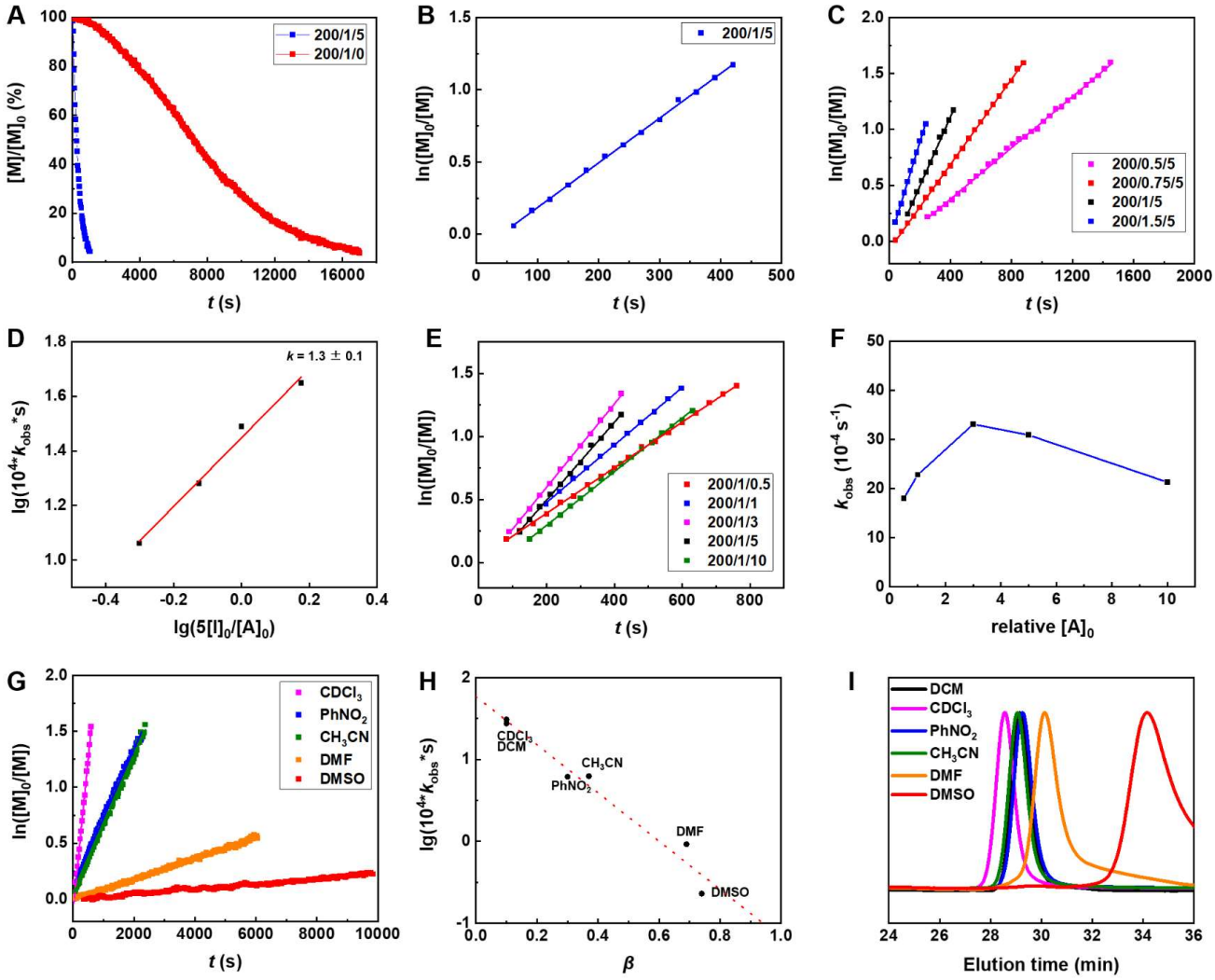

Figure 3. Kinetic study and solvent effect of carboxylic acid-catalyzed ROP of Sar-NCA. (A) Kinetic plots of [M]/[M]$_0$ versus time, with or without the catalyst of benzoic acid at the [M]$_0$/[I]$_0$ ratio of 200/1. (B) Kinetic plot of ln([M]$_0$/[M]) versus time at the [M]$_0$/[I]$_0$/[A]$_0$ ratio of 200/1/5. (C) Kinetic plots of ln([M]$_0$/[M]) versus time with varied initiator equivalent at the [M]$_0$/[A]$_0$ ratio of 200/5. (D) Plot of k_{obs} obtained from (C) versus [I]$_0$ and the linear fitting (red line, R^2 = 0.988) of the data. (E) Kinetic plots of ln([M]$_0$/[M]) versus time with varied [A]$_0$ equivalent at the [M]$_0$/[I]$_0$ ratio of 200/1. (F) Plot of k_{obs} obtained from (E) versus [A]$_0$. (G) Kinetic plots of ln([M]$_0$/[M]) versus time at the [M]$_0$/[I]$_0$/[A]$_0$ ratio of 200/1/5 in different solvents. (H) Plot of k_{obs} obtained from (G) versus β. (I) SEC curves of pSar synthesized in different solvents.

2.2 Influence of carboxylic acidity on Sar-NCA ROP

Next, various carboxylic acids with different acidities were explored for the ROP of Sar-NCA at a fixed $[M]_0/[I]_0/[A]_0$ ratio of 200/1/5 (Figure 4). Despite the difference in chemical structure, all the acid catalysts rendered first-order kinetics of the ROP against monomer, from which k_{obs} were calculated (Figure 4A, Figure S5). Interestingly, a good linear correlation ($R^2 = 0.994$) between k_{obs} and the p*K*a[60] of carboxylic acids was found——the weaker the acidity, the higher the k_{obs} (Figure 4B). Among the acids studied, pivalic acid showed the highest k_{obs}, reaching $(100.6 \pm 1.3) \times 10^{-4}$ s^{-1}, 3 times that of benzoic acid, and more than 50 times that of the acid-free control group. Moreover, all pSar synthesized by carboxylic acid-catalyzed ROP showed symmetrical and narrow SEC peaks, in sharp contrast with the ROP without acid exhibiting significant tailing in the SEC trace (Figure 4C). We speculated that the reason for the rate decrease by the higher acidity of carboxylic acid catalysts (Figure 4B) was essentially the same as the rate inhibition with excessive $[A]_0$ (Figure 3F).

A

entry	acid	pKa (water)	k_{obs} (10^{-4} s^{-1})	M_n^{obt} (kDa)	$Đ$
1	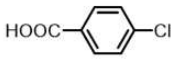	3.99	15.3±0.1	15.5	1.05
2	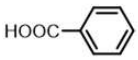	4.20	30.9±0.3	17.5	1.01
3	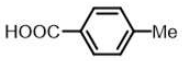	4.37	50.2±0.4	15.3	1.05
4	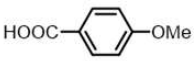	4.47	54.5±0.7	15.9	1.04
5	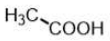	4.76	77.9±0.9	16.2	1.06
6	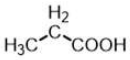	4.87	86.4±1.0	15.5	1.05
7	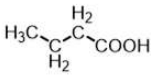	4.82	86.7±1.0	15.8	1.04
8		5.05	100.6±1.3	14.7	1.03
9	none	-	1.95 ± 0.02	12.7	1.07

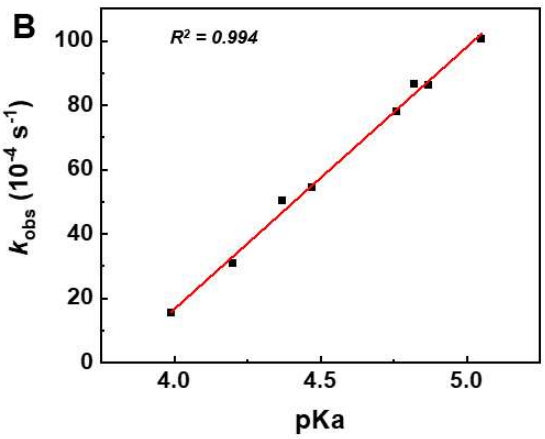

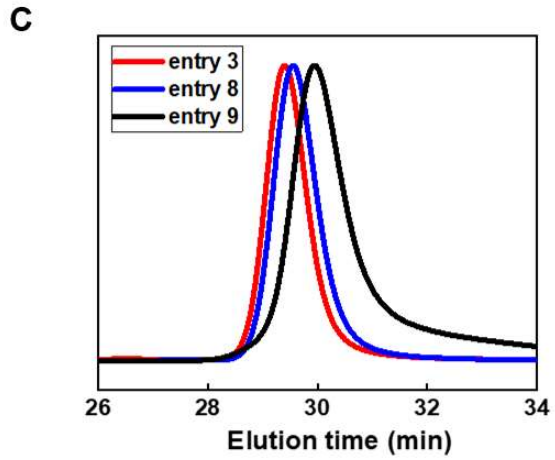

Figure 4. ROP of Sar-NCA catalyzed by different acids. (A) Results of Sar-NCA ROP catalyzed by different carboxylic acids. (B) Plot of k_{obs} versus pKa values of acids. (C) SEC curves of selected entries from (A).

2.3 Pivalic acid-catalyzed consecutive chain extensions for the synthesis of ultra-high molecular weight (UHMW) pSar

Based on the above screening, we identified pivalic acid as a more efficient catalyst than benzoic acid, which could potentially further boost the polymerization kinetics and lead to the construction of pSar with higher MWs. To this end, consecutive chain extensions, each with 2000 equivalent of Sar-NCA relative to the initiator, were conducted (Figure 5A). IR monitoring indicated that it took only 2 h for the first two feeds to reach full monomer conversion, and the third feed required a slightly longer time of 4 h. The last feed needed overnight reaction to consume all monomers. SEC characterization showed that each chain extension led to an overall

shift of the chromatogram peak curve to high MW region (Figure 5B). A UHMW pSar with a 586 kDa MW (DP ~ 8200, $Đ$ = 1.25) was obtained, in good agreement with the theoretical MW and 16 times higher than the previous highest record. (Figure 5C).

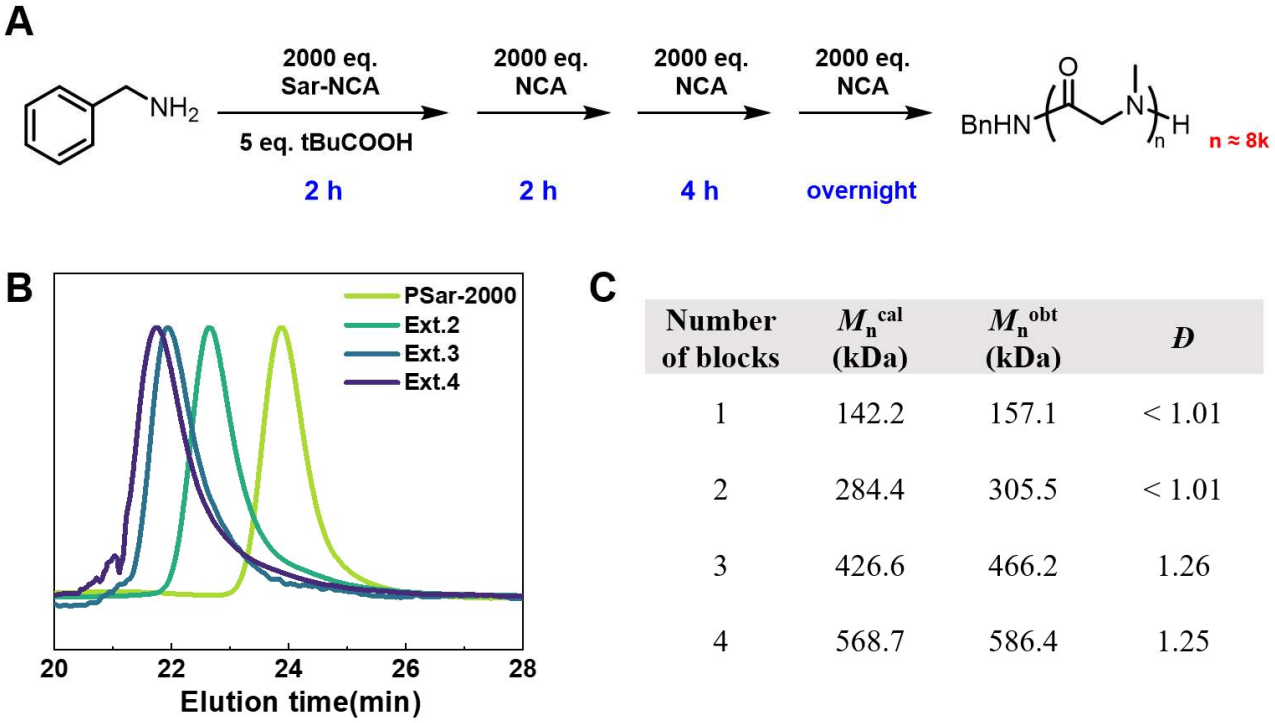

C

Number of blocks	M_n^{cal} (kDa)	M_n^{obt} (kDa)	$Đ$
1	142.2	157.1	< 1.01
2	284.4	305.5	< 1.01
3	426.6	466.2	1.26
4	568.7	586.4	1.25

Figure 5. Chain extension catalyzed by tBuCOOH for the synthesis of high-molecular-weight pSar. (A) Consecutive chain extension experiment. (B) SEC traces of chain extension products. (C) M_n and $Đ$ of pSar products calculated from SEC.

2.4 Mechanism study on carboxylic acid-catalyzed ROP of Sar-NCA

To understand the acceleration mechanism brought by carboxylic acids, DFT calculations were performed based on model chain propagation reactions between Sar-NCA and dimethylamine, the equivalent of the living chain end (Figure 6). For both the non-catalyzed and the acetic acid (AcOH)-catalyzed systems, the ring-opening step could proceed similarly in a stepwise fashion involving the classical nucleophilic addition-elimination process via a tetrahedral intermediate,

or through a concerted mechanism in one elementary reaction (Figure 6A, Path A&B).[40,47,61] For the uncatalyzed system, DFT calculations revealed a favorable result of the concerted pathway over the stepwise pathway, with the activation free energy ($\Delta G^{\ddagger}$) of 20.1 (TSb1) and 36.0 (TSa1) kcal/mol, respectively (Figure 6B and Figure S6). For the acid-catalyzed system (Figure 6A, path C), the introduction of a carboxylic acid catalyst distinctly reshaped the potential energy surface (PES) in the stepwise route, yielding a substantially lower energy barrier $\Delta G^{\ddagger}$ of only 11.4 kcal/mol (Figure 6B). Remarkably, AcOH played a crucial role as a bifunctional catalyst throughout the ring-opening process. In TSc1, the hydrogen bonding between the carbonyl lone pair of AcOH and dimethylamine enhances the nucleophilicity of the amine; in the meantime, the transferring carboxylic proton stabilizes the developing negative charge on the oxygen atom of the NCA carbonyl being attacked. After the formation of the unstable intermediate INTc1, it undergoes a low-barrier proton transfer (TSc2) to give the neutral tetrahedral intermediate complex INTc2 stabilized with AcOH hydrogen bonding. To facilitate the subsequent elimination, AcOH and tetrahedral intermediate then change their hydrogen bonding mode to obtain INTc3 with a slightly higher energy. Next, in INTc3, the carbonyl oxygen and acidic hydrogen of AcOH combine with the hydroxyl and the leaving carboxyl oxygen, respectively, and simultaneously activate the elimination-driven hydroxyl oxygen lone pair and leaving group, preparing for the next elimination transition state TSc3. TSc3, without proton transfer, was also the rate-determining TS (11.4 kcal/mol) for the whole ring-opening stage, being 24.6 and 8.7 kcal/mol lower than stepwise and concerted pathways without acid catalysis. After several consecutive low-barrier TS and INT, the carbamic acid intermediate M1 was produced, and the catalyst AcOH was regenerated. The TS for the acid-catalyzed concerted pathway (Figure 6A, path D), however, could not be located.

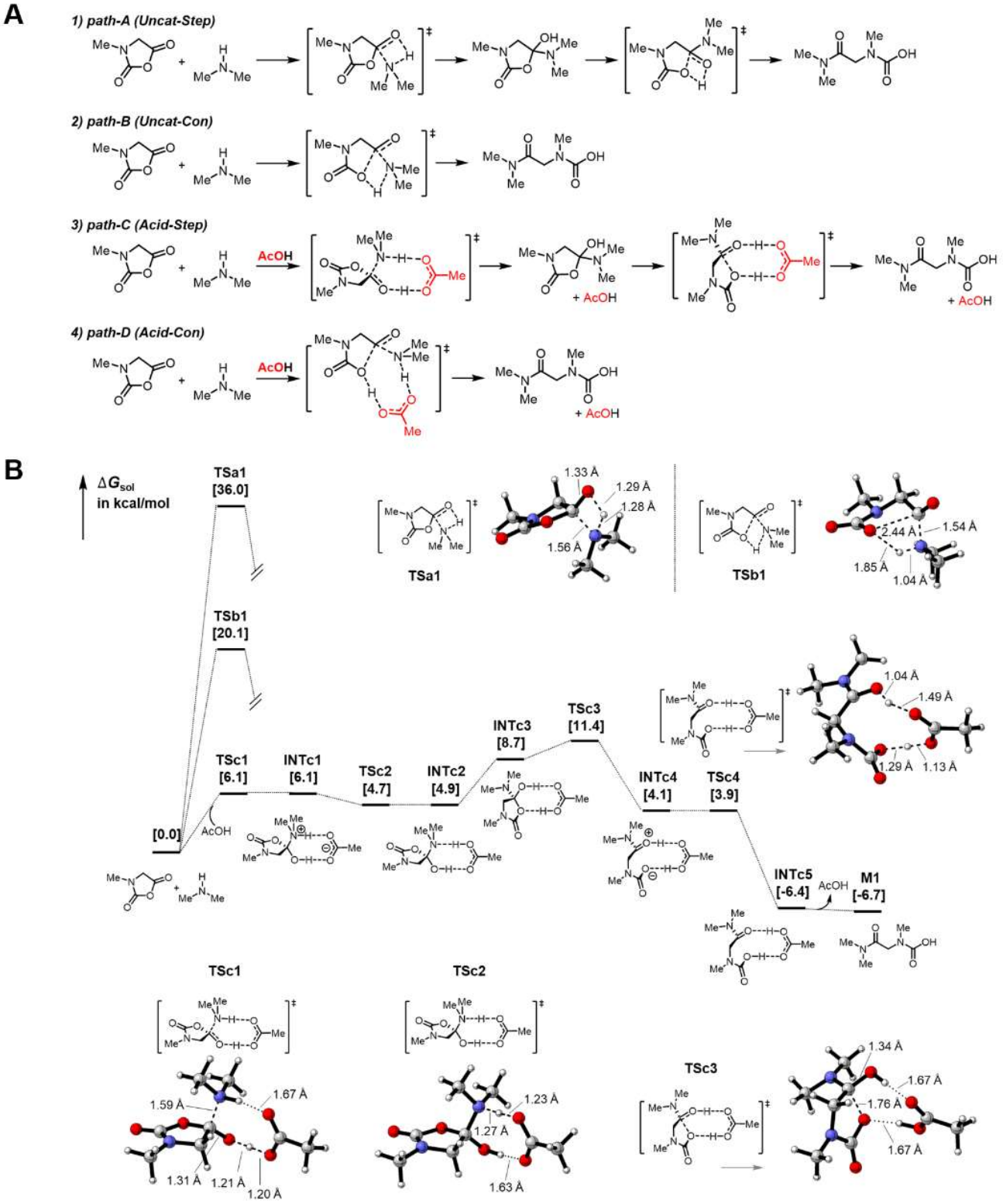

Figure 6. Proposed reaction pathways (A) and computed PES (B) for ring-opening step.

For decarboxylation, the noncatalyzed intramolecular route and the acid-assisted intermolecular proton transfer route were examined by DFT calculation (Figure 7A). The free energy of the highly strained four-member-ring TSa2 was calculated as 30.6 kcal/mol, which corresponds to an unfavored energy barrier $\Delta G^{\ddagger}$ of 37.3 kcal/mol starting from M1. With the catalysis of AcOH, however, the decarboxylation proceeded through a concerted eight-membered-ring TS (TSc5) with the ∠N-H-O and ∠O-H-O being 176.4° and 174.1°, respectively. Compared with TSa2 with a ∠N-H-O of 112.4°, the near linear proton transfer geometry of TSc5 was more favorable, which likely rendered the latter with a significantly reduced $\Delta G^{\ddagger}$ (13.4 kcal/mol). It is worth mentioning that the energy of the decarboxylated intermediate M2 was calculated significantly higher than that of M1 with a carbamic acid (3.0 vs. -6.7 kcal/mol). This result implied that M1, as a resting state or dormant species, was more likely the stable form of the chain end. This theoretical prediction was then supported by in situ NMR experiments. In a sealed NMR tube filled with 1 atm of CO_2, the deuterated DCM solution of *N*,*N*-dimethyl-2-(methylamino)acetamide (M2) was equilibrated for 20 h. In both ^{1}H and ^{13}C NMR spectra, the complete disappearance of M2 signals and the formation of carbamate product M1 were clearly observed (Figure 7B&C).

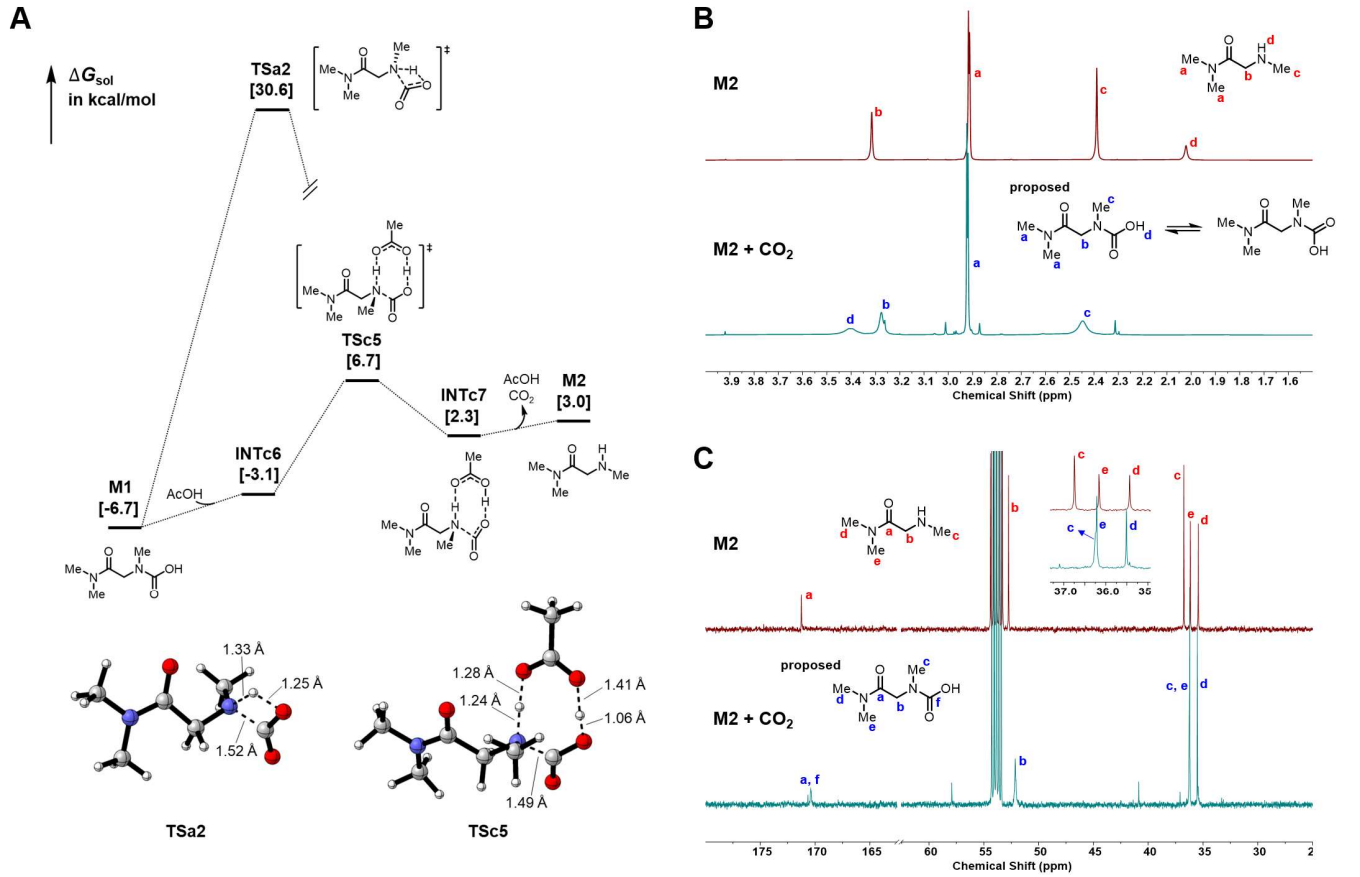

Figure 7. (A) Computed PES for pathways of decarboxylation step. (B) ^{1}H NMR and (C) ^{13}C NMR spectra of M2 before and after equilibration with CO_2.

Taking together the DFT and experimental results, we proposed the following catalytic cycle of the carboxylic acid-enhanced ROP of Sar-NCA (Figure 8). Carbamic acid was the predominant dormant state of the living center. Under the catalysis of carboxylic acid, a molecule of CO_2 was reversibly released through the concerted proton transfer TS, producing the chain propagating species secondary amine. Subsequently, the nucleophilic addition of secondary amines to Sar-NCA led to the tetrahedral intermediate, whose elimination is the RDS for the overall chain growth process. In the elimination TS, the proton of the carboxylic acid binds to the leaving carboxyl group and the carbonyl oxygen binds to the hydroxyl group, simultaneously activating the lone pair and the leaving group for facilitated elimination. After elimination, new carbamic acid species were generated, waiting for the start of a new catalytic cycle. Note that both the

decarboxylation and nucleophilic addition step were thermodynamically unfavored under standard conditions, the irreversible CO_2 escape and the successive ring-opening step forming a stable amide bond seemed to be the critical driving forces of the ROP (see detailed discussion in SI).

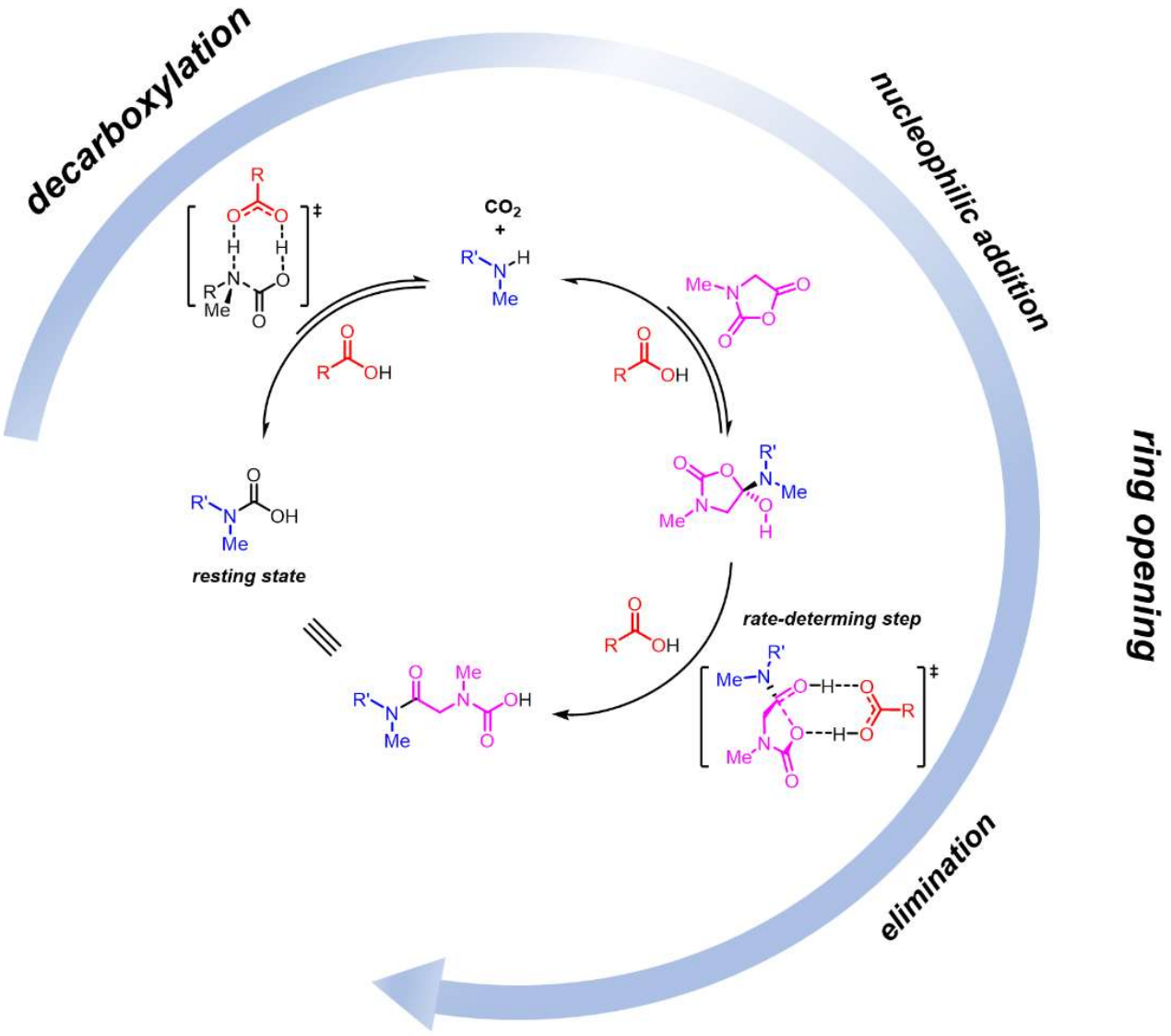

Figure 8. Proposed mechanism for ROP of Sar-NCA catalyzed by carboxylic acids.

2.5 Molecular weight-dependent thermal and mechanical properties of pSar

The thermal and mechanical properties of pSar were examined, which was rarely explored before.

With the ability to obtain UHMW pSar, here, we synthesized pSar samples on gram scales with targeted DP of 500, 2000, and 5000, respectively (Table S4), and paid special attentions on the MW-dependent performances. The 5% weight loss thermal decomposition temperature (T_d), measured by thermogravimetric analysis (TGA), of $pSar_{500}$ and $pSar_{5000}$ was 315 and 339 °C, respectively (Figure 9A), both significantly higher than 250 °C, the previously reported number of $pSar_{100}$.[62] The glass transition temperature (T_g), determined with differential scanning calorimetry (DSC), of $pSar_{500}$ and $pSar_{5000}$ was measured to be 143 and 149 °C, respectively (Figure 9B), similar to the 143 °C value reported in literature. All $pSar_{500}$, $pSar_{2000}$, and $pSar_{5000}$ samples were soluble in water at a concentration greater than or equal to 100 mg/mL. Using the solution casting method, pSar of the above MWs were fabricated into transparent, smooth, thin films, as well as other shaped bulk materials with excellent flexibility (Figure 9C-E). The pSar films exhibited good mechanical strength in uniaxial tensile experiments (Figure 9F-I), with a characteristic MW-dependence on both the ultimate tensile strength and Young's modulus (Figure 9F). Specifically, the $pSar_{5000}$ samples gave an ultimate tensile strength of (60.2 ± 3.0) MPa and Young's modulus of (3.0 ± 0.5) GPa, both greater than those of $pSar_{500}$ and $pSar_{2000}$ (Figure 9F). Interestingly, the mechanical properties of all pSar films showed moisture responsiveness in a 70% humidity environment, with decreased ultimate tensile strengths but markedly increased elongations at break (Figure S10). Additionally, the bending fatigue behavior of $pSar_{5000}$ film was roughly probed by manually bending the film continuously for 40 times, through which no significant failure was observed, demonstrating good fatigue properties (supplementary video). Moreover, pSar could be alternatively manufactured through the thermoforming process under 195 °C to form shaped bulk materials (Figure S11). In summary, the increase in MW greatly improves the thermal stability and mechanical strength of pSar bulk materials, laying the

foundation for the subsequent development of pSar-based materials.

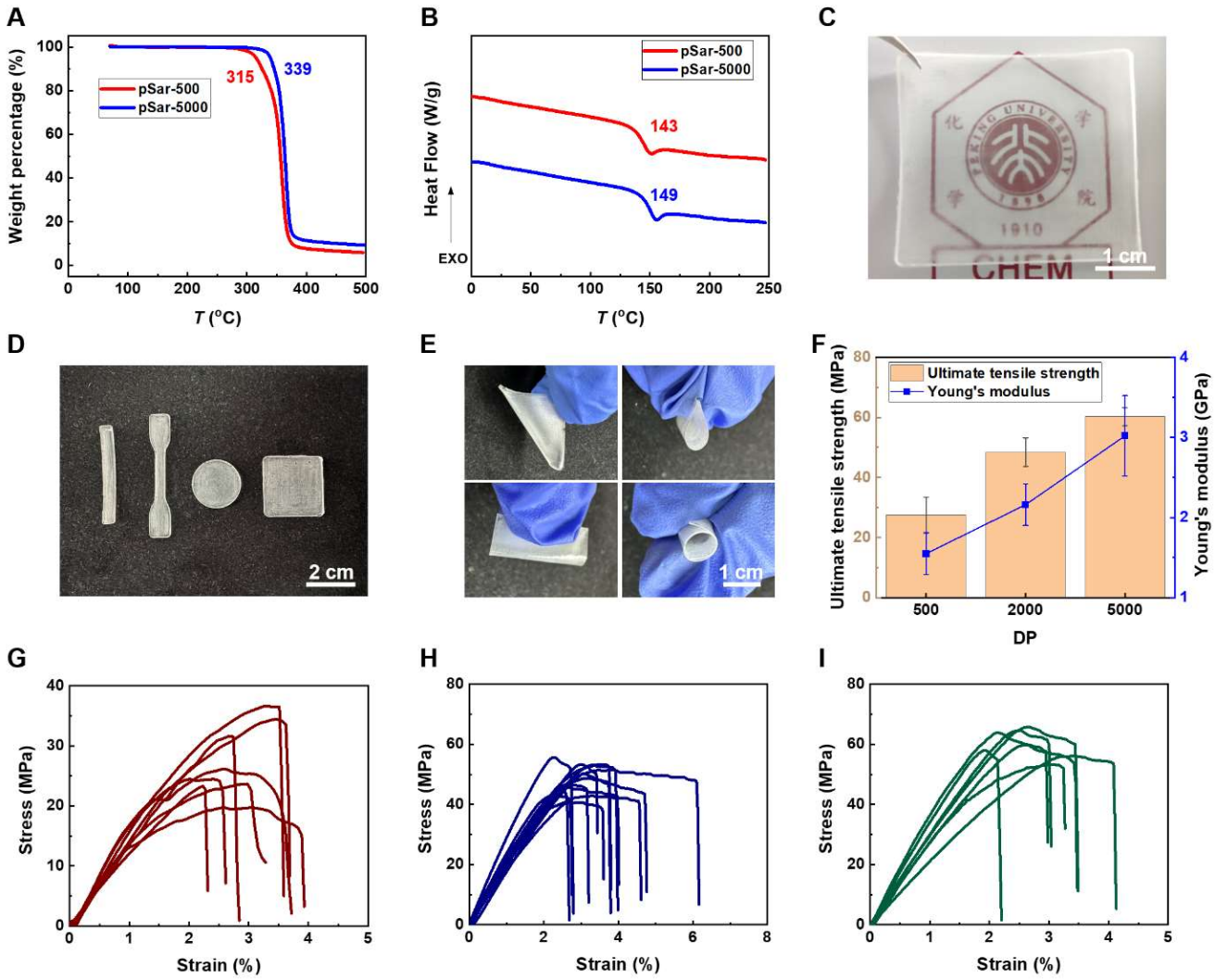

Figure 9. Material properties of HMW pSar. (A) TGA curves of $pSar_{500}$ and $pSar_{5000}$. (B) DSC curves of $pSar_{500}$ and $pSar_{5000}$. (C) Photograph of $pSar_{5000}$ as a transparent film (4.0 cm × 3.5 cm × 92 μm). (D) Shaped pSar bulk materials produced by solution casting. (E) pSar films under bending. (F) Dependence of ultimate tensile strengths and Young's modulus of pSar films on DP. (G)Tensile stress-strain curves of $pSar_{500}$. (H)Tensile stress-strain curves of $pSar_{2000}$. (G)Tensile stress-strain curves of $pSar_{5000}$.

3. Conclusion

This paper reported the controlled/living polymerization of Sar-NCA using carboxylic acids as the catalyst under mild conditions. The method features in fast kinetics up to 50-fold enhancement compared with no acid catalysis, capability of multiple chain extensions, narrow $Đ$ below 1.02,

and UHMW of pSar with obtainable DP up to 8000, 16-fold higher than the current record DP of pSar ever reported. The method also showed good moisture tolerance with no need of air-free conditions or dry solvents for pSar with a targeting DP of 1000 or lower. DFT calculations and experiments elucidated the role of carboxylic acid in the ROP, identifying the carbamic acid as the dormant species before generating the secondary amine for chain propagation. Carboxylic acid was found to facilitate ROP throughout the nucleophilic addition, elimination (breaking C-O bond, RDS), and decarboxylation steps. More specifically, by mainly serving as both hydrogen bond donor and acceptor, the introduction of carboxylic acid enabled the proton transfer via more favorable geometries and reduced charge separation of these processes, thereby lowering the energy barrier significantly. High-molecular-weight pSar exhibited enhanced thermal and mechanical properties superior to its low-molecular-weight counterparts, and can be easily processed. This work greatly enriched the basic understanding of Sar-NCA polymerization, highlighted the importance of proton transfer for NCA ROP in general, and provided a simple yet highly practical route to pSar of various MW and for diverse applications.

ASSOCIATED CONTENT

Supporting Information

The Supporting Information is available free of charge at https://pubs.acs.org/doi/xxx

Materials, instrumentation, experimental methods, and supplementary data (PDF)

Supplementary video (MP4)

AUTHOR INFORMATION

Corresponding Author

Hua Lu − *Beijing National Laboratory for Molecular Sciences, Center for Soft Matter Science and Engineering, Key Laboratory of Polymer Chemistry and Physics of Ministry of Education, College of Chemistry and Molecular Engineering, Peking University, Beijing 100871, China*; orcid.org/0000-0003-2180-3091; Email: chemhualu@pku.edu.cn

Authors

Shuo Wang − *Beijing National Laboratory for Molecular Sciences, Center for Soft Matter Science and Engineering, Key Laboratory of Polymer Chemistry and Physics of Ministry of Education, College of Chemistry and Molecular Engineering, Peking University, Beijing 100871, China*; orcid.org/0000-0002-1380-5890

Ming-Yuan Lu − *Beijing National Laboratory for Molecular Sciences, Center for Soft Matter Science and Engineering, Key Laboratory of Polymer Chemistry and Physics of Ministry of Education, College of Chemistry and Molecular Engineering, Peking University, Beijing 100871, China*

Si-Kang Wan − *Engineering Research Center of Advanced Rare Earth Materials (Ministry of Education), Department of Chemistry, Tsinghua University, 100084 Beijing, China*

Chun-Yan Lyu − *Beijing National Laboratory for Molecular Sciences, Center for Soft Matter Science and Engineering, Key Laboratory of Polymer Chemistry and Physics of Ministry of Education, College of Chemistry and Molecular Engineering, Peking University, Beijing 100871, China*

Zi-You Tian − *Beijing National Laboratory for Molecular Sciences, Center for Soft Matter Science and Engineering, Key Laboratory of Polymer Chemistry and Physics of Ministry of Education, College of Chemistry and Molecular Engineering, Peking University, Beijing 100871, China*

Kai Liu − *Engineering Research Center of Advanced Rare Earth Materials (Ministry of Education), Department of Chemistry, Tsinghua University, 100084 Beijing, China*

Notes

The authors declare no competing financial interest.

ACKNOWLEDGMENTS

This work was supported by National Natural Science Foundation of China (22125101), Beijing Natural Science Foundation (2220023), and Li Ge-Zhao Ning Life Science Youth Research Fund.

REFERENCE

1. Birke, A.; Ling, J.; Barz, M. Polysarcosine-containing copolymers: Synthesis, characterization, self-assembly, and applications. *Prog. Polym. Sci.* **2018**, *81*, 163-208.
2. Weber, B.; Birke, A.; Fischer, K.; Schmidt, M.; Barz, M. Solution Properties of Polysarcosine: From Absolute and Relative Molar Mass Determinations to Complement Activation. *Macromolecules* **2018**, *51*, 2653-2661.
3. Lau, K. H. A.; Ren, C.; Sileika, T. S.; Park, S. H.; Szleifer, I.; Messersmith, P. B. Surface-Grafted Polysarcosine as a Peptoid Antifouling Polymer Brush. *Langmuir* **2012**, *28*, 16099-16107.
4. Hu, Y.; Hou, Y.; Wang, H.; Lu, H. Polysarcosine as an Alternative to PEG for Therapeutic Protein Conjugation. *Bioconjugate Chem.* **2018**, *29*, 2232-2238.
5. Nogueira, S. S.; Schlegel, A.; Maxeiner, K.; Weber, B.; Barz, M.; Schroer, M. A.; Blanchet, C. E.; Svergun, D. I.; Ramishetti, S.; Peer, D.; Langguth, P.; Sahin, U.; Haas, H. Polysarcosine-Functionalized Lipid Nanoparticles for Therapeutic mRNA Delivery. *ACS Appl. Nano Mater.* **2020**, *3*, 10634-10645.
6. Bi, D.; Unthan, D. M.; Hu, L.; Bussmann, J.; Remaut, K.; Barz, M.; Zhang, H. Polysarcosine-based lipid formulations for intracranial delivery of mRNA. *J. Controlled Release* **2023**, *356*, 1-13.
7. Kidchob, T.; Kimura, S.; Imanishi, Y. Amphiphilic poly(Ala)-b-poly(Sar) microspheres loaded with hydrophobic drug. *J. Controlled Release* **1998**, *51*, 241-248.
8. Makino, A.; Kizaka-Kondoh, S.; Yamahara, R.; Hara, I.; Kanzaki, T.; Ozeki, E.; Hiraoka, M.; Kimura, S. Near-infrared fluorescence tumor imaging using nanocarrier composed of poly(l-lactic acid)-block-poly(sarcosine) amphiphilic polydepsipeptide. *Biomaterials* **2009**, *30*, 5156-5160.
9. Birke, A.; Huesmann, D.; Kelsch, A.; Weilbächer, M.; Xie, J.; Bros, M.; Bopp, T.; Becker, C.; Landfester, K.; Barz, M. Polypeptoid-block-polypeptide Copolymers: Synthesis, Characterization, and Application of Amphiphilic Block Copolypept(o)ides in Drug Formulations and Miniemulsion Techniques. *Biomacromolecules* **2014**, *15*, 548-557.
10. Deng, Y.; Zou, T.; Tao, X.; Semetey, V.; Trepout, S.; Marco, S.; Ling, J.; Li, M.-H. Poly(ε-caprolactone)-block-polysarcosine by Ring-Opening Polymerization of Sarcosine N-Thiocarboxyanhydride: Synthesis and Thermoresponsive Self-Assembly. *Biomacromolecules* **2015**, *16*, 3265-3274.
11. Miao, Y.; Xie, F.; Cen, J.; Zhou, F.; Tao, X.; Luo, J.; Han, G.; Kong, X.; Yang, X.; Sun, J.; Ling, J. Fe3+@polyDOPA-b-polysarcosine, a T1-Weighted MRI Contrast Agent via Controlled NTA Polymerization. *ACS Macro Lett.* **2018**, *7*, 693-698.

12. Varlas, S.; Georgiou, P. G.; Bilalis, P.; Jones, J. R.; Hadjichristidis, N.; O'Reilly, R. K. Poly(sarcosine)-Based Nano-Objects with Multi-Protease Resistance by Aqueous Photoinitiated Polymerization-Induced Self-Assembly (Photo-PISA). *Biomacromolecules* **2018**, *19*, 4453-4462.
13. Bauer, T. A.; Imschweiler, J.; Muhl, C.; Weber, B.; Barz, M. Secondary Structure-Driven Self-Assembly of Thiol-Reactive Polypept(o)ides. *Biomacromolecules* **2021**, *22*, 2171-2180.
14. Kincaid, J. R. A.; Wong, M. J.; Akporji, N.; Gallou, F.; Fialho, D. M.; Lipshutz, B. H. Introducing Savie: A Biodegradable Surfactant Enabling Chemo- and Biocatalysis and Related Reactions in Recyclable Water. *J. Am. Chem. Soc.* **2023**, *145*, 4266-4278.
15. Kricheldorf, H. R.; von Lossow, C.; Schwarz, G. Primary Amine-Initiated Polymerizations of Alanine-NCA and Sarcosine-NCA. *Macromol. Chem. Phys.* **2004**, *205*, 918-924.
16. Fetsch, C.; Grossmann, A.; Holz, L.; Nawroth, J. F.; Luxenhofer, R. Polypeptoids from N-Substituted Glycine N-Carboxyanhydrides: Hydrophilic, Hydrophobic, and Amphiphilic Polymers with Poisson Distribution. *Macromolecules* **2011**, *44*, 6746-6758.
17. Doriti, A.; Brosnan, S. M.; Weidner, S. M.; Schlaad, H. Synthesis of polysarcosine from air and moisture stable N-phenoxycarbonyl-N-methylglycine assisted by tertiary amine base. *Polym. Chem.* **2016**, *7*, 3067-3070.
18. Salas-Ambrosio, P.; Tronnet, A.; Since, M.; Bourgeade-Delmas, S.; Stigliani, J.-L.; Vax, A.; Lecommandoux, S.; Dupuy, B.; Verhaeghe, P.; Bonduelle, C. Cyclic Poly(α-peptoid)s by Lithium bis(trimethylsilyl)amide (LiHMDS)-Mediated Ring-Expansion Polymerization: Simple Access to Bioactive Backbones. *J. Am. Chem. Soc.* **2021**, *143*, 3697-3702.
19. Chen, K.; Wu, Y.; Wu, X.; Zhou, M.; Zhou, R.; Wang, J.; Xiao, X.; Yuan, Y.; Liu, R. Facile synthesis of polypeptoids bearing bulky sidechains via urea accelerated ring-opening polymerization of α-amino acid N-substituted N-carboxyanhydrides. *Polym. Chem.* **2022**, *13*, 420-426.
20. Rasines Mazo, A.; Allison-Logan, S.; Karimi, F.; Chan, N. J.-A.; Qiu, W.; Duan, W.; O'Brien-Simpson, N. M.; Qiao, G. G. Ring opening polymerization of α-amino acids: advances in synthesis, architecture and applications of polypeptides and their hybrids. *Chem. Soc. Rev.* **2020**, *49*, 4737-4834.
21. Hadjichristidis, N.; Iatrou, H.; Pitsikalis, M.; Sakellariou, G. Synthesis of Well-Defined Polypeptide-Based Materials via the Ring-Opening Polymerization of α-Amino Acid N-Carboxyanhydrides. *Chem. Rev.* **2009**, *109*, 5528-5578.
22. Deming, T. J. Facile synthesis of block copolypeptides of defined architecture. *Nature* **1997**, *390*, 386-389.
23. Dimitrov, I.; Schlaad, H. Synthesis of nearly monodisperse polystyrene–polypeptide block copolymers via polymerisation of N-carboxyanhydrides. *Chem. Commun.* **2003**, 2944-2945.
24. Lu, H.; Cheng, J. Hexamethyldisilazane-Mediated Controlled Polymerization of α-Amino Acid N-Carboxyanhydrides. *J. Am. Chem. Soc.* **2007**, *129*, 14114-14115.
25. Conejos-Sánchez, I.; Duro-Castano, A.; Birke, A.; Barz, M.; Vicent, M. J. A controlled and versatile NCA polymerization method for the synthesis of polypeptides. *Polym. Chem.* **2013**, *4*, 3182-3186.
26. Zhao, W.; Lv, Y.; Li, J.; Feng, Z.; Ni, Y.; Hadjichristidis, N. Fast and selective organocatalytic ring-opening polymerization by fluorinated alcohol without a cocatalyst. *Nat. Commun.* **2019**, *10*, 3590.
27. Song, Z.; Fu, H.; Wang, J.; Hui, J.; Xue, T.; Pacheco, L. A.; Yan, H.; Baumgartner, R.; Wang, Z.; Xia, Y.; Wang, X.; Yin, L.; Chen, C.; Rodríguez-López, J.; Ferguson, A. L.; Lin, Y.; Cheng, J. Synthesis of polypeptides via bioinspired polymerization of in situ purified *N*-carboxyanhydrides. *Proc. Natl. Acad. Sci. U.S.A.* **2019**, *116*, 10658-10663.
28. Wu, Y.; Chen, K.; Wu, X.; Liu, L.; Zhang, W.; Ding, Y.; Liu, S.; Zhou, M.; Shao, N.; Ji, Z.; Chen, J.; Zhu, M.; Liu, R. Superfast and Water-Insensitive Polymerization on α-Amino Acid N-Carboxyanhydrides to Prepare Polypeptides Using Tetraalkylammonium Carboxylate as the Initiator. *Angew. Chem., Int. Ed.* **2021**, *60*, 26063-26071.
29. Li, K.; Li, Z.; Shen, Y.; Fu, X.; Chen, C.; Li, Z. Organobase 1,1,3,3-tetramethyl guanidine catalyzed rapid ring-opening polymerization of α-amino acid N-carboxyanhydrides adaptive to amine, alcohol and carboxyl acid initiators. *Polym. Chem.* **2022**, *13*, 586-591.
30. Lv, W.; Wang, Y.; Li, M.; Wang, X.; Tao, Y. Precision Synthesis of Polypeptides via Living Anionic Ring-Opening Polymerization of N-Carboxyanhydrides by Tri-thiourea Catalysts. *J. Am. Chem. Soc.* **2022**, *144*, 23622-23632.

31. Kricheldorf, H. R.; Sell, M.; Schwarz, G. Primary Amine‐Initiated Polymerizations of α‐Amino Acid N‐Thiocarbonic Acid Anhydrosulfide. *J. Macromol. Sci., Part A: Pure Appl. Chem.* **2008**, *45*, 425-430.
32. Tao, X.; Zheng, B.; Kricheldorf, H. R.; Ling, J. Are N-substituted glycine N-thiocarboxyanhydride monomers really hard to polymerize? *J. Polym. Sci. Part A: Polym. Chem.* **2017**, *55*, 404-410.
33. Tao, X.; Zheng, B.; Bai, T.; Li, M.-H.; Ling, J. Polymerization of N-Substituted Glycine N-Thiocarboxyanhydride through Regioselective Initiation of Cysteamine: A Direct Way toward Thiol-Capped Polypeptoids. *Macromolecules* **2018**, *51*, 4494-4501.
34. Zheng, B.; Xu, S.; Ni, X.; Ling, J. Understanding Acid-Promoted Polymerization of the N-Substituted Glycine N-Thiocarboxyanhydride in Polar Solvents. *Biomacromolecules* **2021**, *22*, 1579-1589.
35. Siefker, D.; Chan, B. A.; Zhang, M.; Nho, J.-W.; Zhang, D. 1,1,3,3-Tetramethylguanidine-Mediated Zwitterionic Ring-Opening Polymerization of Sarcosine-Derived N-Thiocarboxyanhydride toward Well-Defined Polysarcosine. *Macromolecules* **2022**, *55*, 2509-2516.
36. Siefker, D.; Williams, A. Z.; Stanley, G. G.; Zhang, D. Organic Acid Promoted Controlled Ring-Opening Polymerization of α-Amino Acid-Derived N-thiocarboxyanhydrides (NTAs) toward Well-defined Polypeptides. *ACS Macro Lett.* **2018**, *7*, 1272-1277.
37. Hou, Y.; Lu, H. Protein PEPylation: A New Paradigm of Protein–Polymer Conjugation. *Bioconjugate Chem.* **2019**, *30*, 1604-1616.
38. Cheng, G.-J.; Zhang, X.; Chung, L. W.; Xu, L.; Wu, Y.-D. Computational Organic Chemistry: Bridging Theory and Experiment in Establishing the Mechanisms of Chemical Reactions. *J. Am. Chem. Soc.* **2015**, *137*, 1706-1725.
39. Scheiner, S. Theoretical studies of proton transfers. *Acc. Chem. Res.* **1985**, *18*, 174-180.
40. Liu, J.; Ling, J. DFT Study on Amine-Mediated Ring-Opening Mechanism of α-Amino Acid N-Carboxyanhydride and N-Substituted Glycine N-Carboxyanhydride: Secondary Amine versus Primary Amine. *J. Phys. Chem. A* **2015**, *119*, 7070-7074.
41. Wang, L.; Zipse, H. Bifunctional Catalysis of Ester Aminolysis - A Computational and Experimental Study. *Liebigs Ann.* **1996**, 1501-1509.
42. Duan, X.; Scheiner, S. Energetics, proton transfer rates, and kinetic isotope effects in bent hydrogen bonds. *J. Am. Chem. Soc.* **1992**, *114*, 5849-5856.
43. Nguyen Minh, T.; Ha, T. K. A theoretical study of the formation of carbonic acid from the hydration of carbon dioxide: a case of active solvent catalysis. *J. Am. Chem. Soc.* **1984**, *106*, 599-602.
44. Williams, I. H.; Spangler, D.; Femec, D. A.; Maggiora, G. M.; Schowen, R. L. Theoretical models for solvation and catalysis in carbonyl addition. *J. Am. Chem. Soc.* **1983**, *105*, 31-40.
45. Williams, I. H. Theoretical modelling of specific solvation effects upon carbonyl addition. *J. Am. Chem. Soc.* **1987**, *109*, 6299-6307.
46. Ilieva, S.; Galabov, B.; Musaev, D. G.; Morokuma, K.; Schaefer, H. F. Computational Study of the Aminolysis of Esters. The Reaction of Methylformate with Ammonia. *J. Org. Chem.* **2003**, *68*, 1496-1502.
47. Petrova, T.; Okovytyy, S.; Gorb, L.; Leszczynski, J. Computational Study of the Aminolysis of Anhydrides: Effect of the Catalysis to the Reaction of Succinic Anhydride with Methylamine in Gas Phase and Nonpolar Solution. *J. Phys. Chem. A* **2008**, *112*, 5224-5235.
48. Hu, Y.; Tian, Z.-Y.; Xiong, W.; Wang, D.; Zhao, R.; Xie, Y.; Song, Y.-Q.; Zhu, J.; Lu, H. Water-Assisted and Protein-Initiated Fast and Controlled Ring-Opening Polymerization of Proline N-Carboxyanhydride. *Natl. Sci. Rev.* **2022**, nwac033.
49. Jehanno, C.; Mezzasalma, L.; Sardon, H.; Ruipérez, F.; Coulembier, O.; Taton, D. Benzoic Acid as an Efficient Organocatalyst for the Statistical Ring-Opening Copolymerization of ε-Caprolactone and L-Lactide: A Computational Investigation. *Macromolecules* **2019**, *52*, 9238-9247.
50. da Silva, G. Carboxylic Acid Catalyzed Keto-Enol Tautomerizations in the Gas Phase. *Angew. Chem., Int. Ed.* **2010**, *49*, 7523-7525.
51. Kim, Y. Direct Dynamics Calculation for the Double Proton Transfer in Formic Acid Dimer. *J. Am. Chem. Soc.* **1996**, *118*, 1522-1528.

52. Lim, J.-H.; Lee, E. K.; Kim, Y. Theoretical Study for Solvent Effect on the Potential Energy Surface for the Double Proton Transfer in Formic Acid Dimer and Formamidine Dimer. *J. Phys. Chem. A* **1997**, *101*, 2233-2239.
53. Feng, G.; Favero, L. B.; Maris, A.; Vigorito, A.; Caminati, W.; Meyer, R. Proton Transfer in Homodimers of Carboxylic Acids: The Rotational Spectrum of the Dimer of Acrylic Acid. *J. Am. Chem. Soc.* **2012**, *134*, 19281-19286.
54. Ballard, D. G. H.; Bamford, C. H. Studies in polymerization -VII. The polymerization of N-carboxy-α-amino acid anhydrides. *Proc. R. Soc. London, Ser. A* **1954**, *223*, 495-520.
55. Wang, S.; Lu, H. Ring-Opening Polymerization of Amino Acid N-Carboxyanhydrides with Unprotected/Reactive Side Groups. I. d-Penicillamine N-Carboxyanhydride. *ACS Macro Lett.* **2023**, *12*, 555-562.
56. Liang, J.; Zhi, X.; Zhou, Q.; Yang, J. Binaphthol-derived phosphoric acids as efficient organocatalysts for the controlled ring-opening polymerization of γ-benzyl- -glutamate N-carboxyanhydrides. *Polymer* **2019**, *165*, 83-90.
57. Kamlet, M. J.; Taft, R. W. The solvatochromic comparison method. I. The .beta.-scale of solvent hydrogen-bond acceptor (HBA) basicities. *J. Am. Chem. Soc.* **1976**, *98*, 377-383.
58. Kamlet, M. J.; Abboud, J. L. M.; Abraham, M. H.; Taft, R. W. Linear solvation energy relationships. 23. A comprehensive collection of the solvatochromic parameters, .pi.*, .alpha., and .beta., and some methods for simplifying the generalized solvatochromic equation. *J. Org. Chem.* **1983**, *48*, 2877-2887.
59. Komarova, A. O.; Dick, G. R.; Luterbacher, J. S. Diformylxylose as a new polar aprotic solvent produced from renewable biomass. *Green Chem.* **2021**, *23*, 4790-4799.
60. Kortüm, G.; Vogel, W.; Andrussow, K. Disssociation constants of organic acids in aqueous solution. *Pure Appl. Chem.* **1960**, *1*, 187-536.
61. Ling, J.; Huang, Y. Understanding the Ring-Opening Reaction of α-Amino Acid N-Carboxyanhydride in an Amine-Mediated Living Polymerization: A DFT Study. *Macromol. Chem. Phys.* **2010**, *211*, 1708-1711.
62. Fetsch, C.; Luxenhofer, R. Thermal Properties of Aliphatic Polypeptoids. *Polymers* **2013**, *5*, 112-127.

For Table of Contents Only